Drift of Sea Ice Ridges in the Pechora Sea

Kenneth Johannessen and Ove Tobias Gudmestad

(*Statoil, Norway*)

Sveinung Løset

(*Norwegian University of Science and Technology*)

The drift of sea ice ridges and hits on an offshore structure with dimensions 200 m by 200 m have been studied for the Dolginskoye oil field in the Pechora Sea. The calculations were made with the computer program ICEBERG. The mean drift speed of the ice ridges was found to be 0·21 m/s with a maximum speed of 0·89 m/s. The expected number of hits per year was calculated to be 737. It was assumed that a total number of 133 000 sea ice ridges would be produced in (or have entered) the Pechora Sea per year. Under the same assumption, the expected number of ridges entering a safety zone around a platform of 1852 m by 1852 m was found to be 5649. However, due to uncertainties concerning the population of ridges, their shapes, sizes, drag coefficients and tidal action, the results should be used with care and only considered as indicative. The ridge drift pattern was predominantly to the northeast in the winter months. A structure located at Dolginskoye will most probably be exposed to sea ice ridges that are formed in the area around Khodovarihka.

KEY WORDS

1. Sea Ice. 2. Simulation. 3. Safety.

1. INTRODUCTION. Sea ice ridges are formed by compression or shear in the ice cover. Normally their thickness exceeds the surrounding sea ice thickness (Timco and Burden, 1996; Høyland and Løset, 1999). Thus the loads these ridges may exert on offshore structures should be considered in the design of such structures. A possible offshore development in the Pechora Sea will require estimates of the physical environmental loads. One part of these investigations will be to examine the drift pattern and speeds of sea ice ridges.

Ice ridges that drift into shallow waters may cause scouring and damage to pipelines and other equipment placed on the seabed. Impact between installations or ships and ice ridges may also cause serious damage and danger of oil spills. The consequence of oil spills in arctic waters could be a major disaster, and concern about the environment must therefore be given a high priority.

The paper starts by briefly explaining the balance of momentum of ice drifting at sea. Thereafter it elaborates on the environmental factors that govern the drift and the implementation of these equations in the computer program ICEBERG. The rest of the paper is devoted to a discussion of the environmental inputs to the simulation and the estimation of hit rates.

2. BALANCE OF MOMENTUM. The drift of icebergs and sea ice ridges is different in that icebergs are exposed to pressure forces from current and wind while

https://doi.org/10.1017/S0373463300001144 Published online by Cambridge University Press

ridges are exposed to both pressure drag and skin friction. Furthermore, icebergs have a much deeper draft than ridges, and this means that the vertical current profile is quite important for the estimation of iceberg drift. However, with this in mind, most of the terms from the theory of iceberg drift can be used when estimating the drift of ice ridges at sea.

To find the movement of an ice ridge at an initially known position, we simply integrate the speed at which the ridge is moving. To find the speed we integrate the acceleration found from Newton's Second Law:

$$M\frac{d\mathbf{V}_i}{dt} = -Mf\mathbf{k}\times\mathbf{V}_i + \mathbf{F}_a + \mathbf{F}_w + \mathbf{F}_r + \mathbf{F}_s + \mathbf{F}_p, \tag{1}$$

where: M is the sum of physical and added mass of the ice ridge, $M = m_i + m_a$, $\frac{d\mathbf{V}_i}{dt}$ is the local acceleration of the ice ridge, $-f\mathbf{k}\times\mathbf{V}_i$ is acceleration due to Coriolis where f is the Coriolis parameter and **k** is the unit vector in vertical direction. The other factors in (1) are: $\mathbf{F}_a$ – air form drag, $\mathbf{F}_w$ – water drag, $\mathbf{F}_r$ – wave radiation force, $\mathbf{F}_s$ – sea ice drag, and $\mathbf{F}_p$ is the horizontal pressure gradient force exerted by the water on the volume that the ice ridge displaces.

3. ENVIRONMENTAL FACTORS

3.1. *Wind.* The air drag force is given by:

$$\mathbf{F}_a = \tfrac{1}{2}\times\rho_a\times C_a\times A_a\times|\mathbf{V}_a-\mathbf{V}_i|(\mathbf{V}_a-\mathbf{V}_i), \tag{2}$$

where: A_a is the cross-section area above the water and normal to the flow, ρ_a is the density of air, C_a is the air drag-coefficient and $|\mathbf{V}_a-\mathbf{V}_i|$ is the absolute relative velocity between air and the ridge.

If the sea is covered with ice, the friction between the ice and the air will cause a force called skin-friction acting on the ice. This force will also depend on the relative velocity between ice and wind and can be expressed as:

$$\mathbf{F}_a = \rho_a\times C_{asf}\times A_{asurf}\times|\mathbf{V}_a-\mathbf{V}_i|(\mathbf{V}_a-\mathbf{V}_i) \tag{3}$$

where: A_{asurf} is the area of the ridge surface/ice flow surface and C_{asf} is the air skin-friction coefficient.

3.2. *Current.* The current comprises several components such as geostrophic current, wind driven current, tidal current and inertial current. The first three of these current components will give a relative velocity between ice ridge and water, $\mathbf{V}_w-\mathbf{V}_i$, and contribute to a water drag force on the ridge. $\mathbf{V}_w$ is the water speed, while $\mathbf{V}_i$ is the ice ridge speed. This drag force will also depend on the water density, ρ_w, the submerged cross-sectional area, A_{wd}, and a water drag coefficient, C_w:

$$\mathbf{F}_w = \tfrac{1}{2}\times\rho_w\times C_w\times A_{wd}\times|\mathbf{V}_w-\mathbf{V}_i|(\mathbf{V}_w-\mathbf{V}_i). \tag{4}$$

4. ICE RIDGE SHAPES.

The shape of ice ridges has been studied by a number of authors. The best overview is probably given by Timco and Burden (1996). Compression or shear in an ice cover forms sea ice ridges, and a typical ridge will consist of a mixture of ice blocks, slush, water and air. The data on ice ridge shapes in the Pechora Sea is sparse. To find the drag forces, the cross-sectional areas normal to the wind and current both above and below the water line must be known.

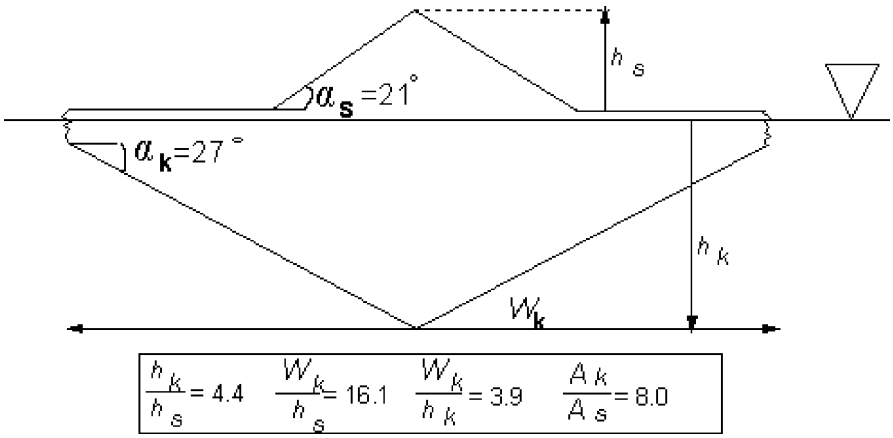

Figure 1. First-year ice ridge: where h_k is the maximum keel depth (m), h_s is the maximum sail height (m), W_k is the keel width (m). Further, A_k is cross sectional area of keel (m^2), A_s is cross sectional area of sail (m^2), a_S is inclination of sail (°), a_K is inclination of keel (°).

The keels and sails of ice ridges usually are much less than for icebergs, while the size of the surface areas may be similar. Also the skin friction must be assumed to have an influence on the drift. Further, the ice ridge mass is needed in order to find the acceleration according to Newton's Second Law (1). To simplify the calculations, a standard ridge shape based on physical observations should be used to find the above mentioned parameters.

Høyland and Løset (1999) observed a ridge that was located in the Van Mijen fjord at Spitsbergen. This ridge was 15 m long, 10 m wide and had a maximum sail height of 1 m. The initial keel depth was 4·4 m.

Timco and Burden (1996) obtained details on 176 ridges from 22 different sources in the Beaufort Sea and temperate waters. Of these, 112 were first-year and 64 multi-year sea ice ridges. From the collection of the data on ridge shapes and sizes, definite relationships were found between several ridge properties. Figure 1 shows the basic element in an 'average' first-year ice ridge.

In the Pechora Sea, the occurrence of first-year ice is predominant, but some multi-year ice ridges will drift from the Kara Sea, through the Kara gate and into the Pechora Sea (Gudmestad *et al*., 1999). Both types of ridges may therefore be expected to appear in these waters.

By comparing the ice ridge observed by Høyland and Løset (1999) with the Timco and Burden (1996) 'average' first-year ice ridge, there seems to be a good agreement between the parameters of the cross-sections. For the lack of better data, we therefore assume that the results from Timco and Burden (1996) can be used in the Pechora Sea. No information was found on drag and added mass coefficients for ice ridges.

5. THE COMPUTER PROGRAM – ICEBERG

5.1. *General*. ICEBERG is a program written in MATLAB™ code that calculates the drift of an ice ridge on the basis of the force exerted by several physical environmental factors. Some explanation of the basics of ICEBERG will be necessary for the reader to understand the calculations performed and the subsequent results. A detailed description of ICEBERG is given in Johannessen (1998).

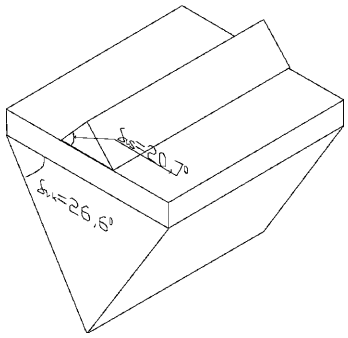

Figure 2. Ice ridge shape used in ICEBERG.

5.2. *Numerical Model.* The ice ridge drift track, $x_i(t)$, is determined by solving the following system of equations:

$$\frac{d\mathbf{x}}{dt} = (\mathbf{V}_i - \mathbf{V}_w) + \mathbf{V}_w, \tag{5}$$

$$M\left(\frac{d(\mathbf{V}_i - \mathbf{V}_w)}{dt}\right) = -Mf\mathbf{k} \times (\mathbf{V}_i - \mathbf{V}_w) + \mathbf{F}_a + \mathbf{F}_w + \mathbf{F}_r + \mathbf{F}_s. \tag{6}$$

where: $\mathbf{F}_a$ is a function of $\mathbf{V}_a - \mathbf{V}_i$, $\mathbf{F}_w$ is a function of $\mathbf{V}_w - \mathbf{V}_i$, $\mathbf{F}_s$ is a function of $\mathbf{V}_s - \mathbf{V}_i$ and $\mathbf{F}_r$ is independent of the velocities. Initial conditions needed to solve equations (5) and (6) are the ice ridge start position and start velocity. All the drag forces in (6) are expressed as functions of relative velocities, and the difference between ice ridge and water velocity is considered as the unknown variable.

The water velocity – $\mathbf{V_w}$, is found by adding the residual current – $\mathbf{V_g}$, the tidal current – $\mathbf{V_{tc}}$, and the wind-induced current – $\mathbf{V_{wi}}$, at the surface. The water drag forces, however, are treated as two separate forces; wind-induced water drag force and drag force from residual and tidal current. This is done because both the direction and the magnitude of the wind-induced current changes with the depth. If updated environmental data is available, for example every 30 minutes, equation (6) can be used to calculate and monitor the drift speed and movement of an ice ridge.

5.3. *Environmental Input and Use of Parameters.*

5.3.1. *Ice Ridge Mass.* Regarding the shapes of the ridges, reference is made to observations by Timco and Burden (1996) as discussed in Section 4. The ice ridge cross-sections have been extrapolated in the third direction (the length) to find an estimate of the ridge masses as shown in Figure 2. The mass is then found from the displaced volume:

$$M_i = A_w \times L \times \rho_w \,[\mathrm{kg}], \tag{7}$$

where: M_i is the ice ridge mass and ρ_w is the density of seawater. A_w is the ice ridge cross-sectional area below the waterline, assumed parallel to the current. Trigonometry and use of the empirical relations given by Timco and Burden (1996), as shown in Figure 1, gives:

$$A_w \approx \left(\frac{h_s^2}{\tan(\alpha_s)} + W_k \times 0{\cdot}1235 \times T_b\right) \times 8{\cdot}8\,[\mathrm{m}^2], \tag{8}$$

where: T_b is the thickness of the consolidated layer, and the constant 0·1235 is found from equation (9) and tells how much of the consolidated layer is above the water

https://doi.org/10.1017/S0373463300001144 Published online by Cambridge University Press

surface (Arntsen *et al*., 1998). The draft of the ice is assumed to be equal to 7·1 times the sail, which means that 12·4% of the consolidated layer will be exposed to wind forces.

$$Draught = \frac{\rho_{ice}}{\rho_{water} - \rho_{ice}} \times Sail[m], \tag{9}$$

W_k is the width of the keel and, according to Timco and Burden (1996), is typically 15·1 times the maximum sail height – h_s. The term in the parenthesis in equation (8) gives the ice ridge cross-section above the water – A_s, and multiplying this with 8·8 will give an estimate of the cross-sectional area below the water surface ($A_w/A_s = 8{\cdot}8$ according to Timco and Burden ,1996).

5.3.2. *Wind Drag*. The wind drag is found by using equation (2) with the following values: A_a is the projected area above the water and normal to the wind. A_a is found by assuming the ridge to drift with its long side normal to incoming wind as shown in Figure 2.

$$A_a = L \times h_s[m^2], \tag{10}$$

where: L is the length of the long side of the ice ridge if it is rectangular as shown in Figure 1. If the surface shape is more circular, the ice-flow diameter will be used rather than the length. Further, h_s is the maximum ice ridge sail height and C_a is the wind drag coefficient recommended by Bigg *et al*. (1996) for icebergs. C_a was derived by Chiriwella and Miller (1978) and Smith (1993), and equals 1·3. The air density $\rho_a$is set equal to 1·25 kg/m^3. The relative velocity between wind and ice ridge speeds is calculated as the wind speed alone since the ice ridge speed normally is very small in comparison and can be neglected. The wind speed and direction are found from the national meterological office (DNMI) hindcast archive.

5.3.3. *Skin Friction*. The skin friction is found by using equation (3), and inserting the following values: A_{asurf} is the surface ridge area above the water where the wind friction acts. Table 1 is found from Losev and Gorbunov (1977), and gives

Table 1. Ice flow area distribution (Losev and Gorbunov, 1977).

Flow area, km^2	0–0·01	0·01–0·03	0·03–0·1	0·1–0·3	0·3–1·0	> 1·0
Prob. of occurrence	23%	6%	10%	10%	20%	31%

the ice-flow area distribution in the Kara Sea. Because of the lack of corresponding information for the Pechora Sea, this distribution is used to define the surface areas in the simulations performed with ICEBERG. The skin friction coefficient $-C_{asf}$ is set to 2×10^{-3}.

5.3.4. *Waves*. The ice ridges are usually surrounded by sea ice, which effectively will quench the waves. The force from waves is therefore be neglected in the simulations.

5.3.5. *Sea Ice*. In the simulations, the sea ice force is set to zero. It is likely that the ice ridges will drift with the sea ice, and not because of it.

5.3.6. *Wind-induced Current*. The wind-induced current is neglected in the ice ridge simulations. This is done because the assumption is made that the polynyas are small compared to the area covered with ice. The wind will mainly act on the ice flows with a skin friction force instead of inducing a water surface current.

5.3.7. *Geostrophic Current*. Slagstad and Wassmann (1995) described a 3-dimensional model that simulates the current field in the Barents Sea. The model uses data input from meteorological stations and data from DNMI hindcast database. The current patterns from this model are implemented in ICEBERG.

5.3.8. *Tidal Current*. The tidal current used in the simulations is found by use of appropriate parameters in Gjevik *et al.* (1990). However, the quality of the model for the Pechora Sea has never been verified.

5.3.9. *Force from Water Current*. The geostrophic current vectors are superimposed with the tidal current vectors and used in the drag formula given in equation (3). The water density – ρ_w, is set equal to 1025 kg/m^3, and the drag coefficient – C_w, is set equal to 0·9. The cross-section area normal to the incident flow- A_{wd}, will be equal to the keel depth multiplied by the ice flow diameter/length. The ridges are assumed to drift with their widest sides normal to the incident currents as shown in Figure 3.

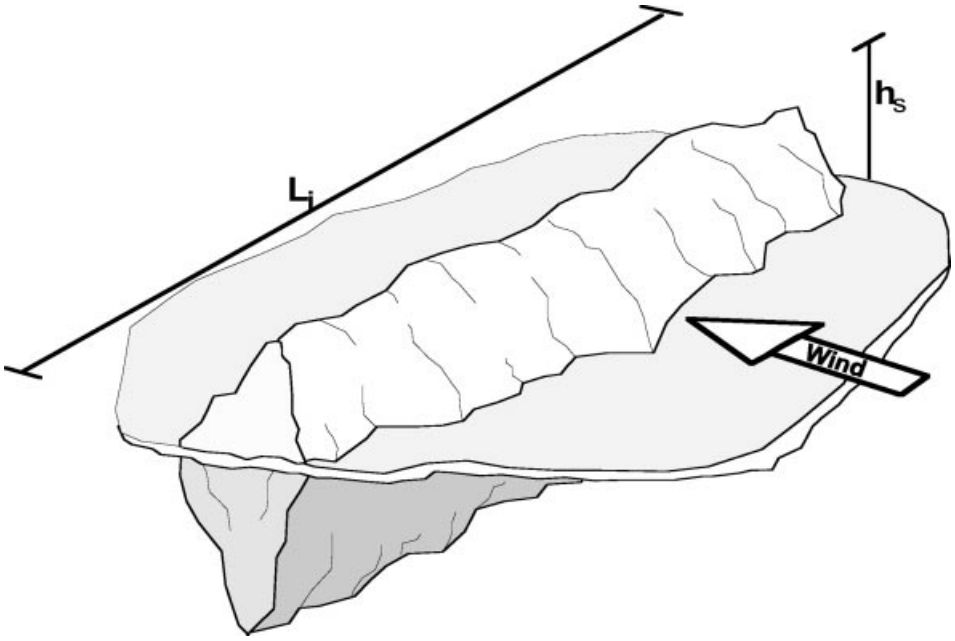

Figure 3. Ice ridge orientation when exposed to wind.

5.3.10. *Coriolis Force*. The Coriolis force is found from the first term on the right-hand side in equation (1) using the following parameters: M – the ice ridge mass, equals the product of displaced volume – ∇, and the water density – ρ_w. The added mass – m_a, is neglected due to entrained melt-water carried along with the ridges (Smith, 1993).

$$M = m_i = 7{\cdot}1 \times Sail \times W_k \times L \times \rho_w [kg], \tag{11}$$

where f is the Coriolis parameter:

$$f = 1{\cdot}45 \times 10^{-4} \times \sin(Ice - ridge\text{-}latitude)\,[\mathrm{rad/s}] \tag{12}$$

6. ICE RIDGE HITS. To determine the risk of an ice ridge hitting a structure located at a certain position, a method described by Mathiesen *et al.* (1992) is used.

https://doi.org/10.1017/S0373463300001144 Published online by Cambridge University Press

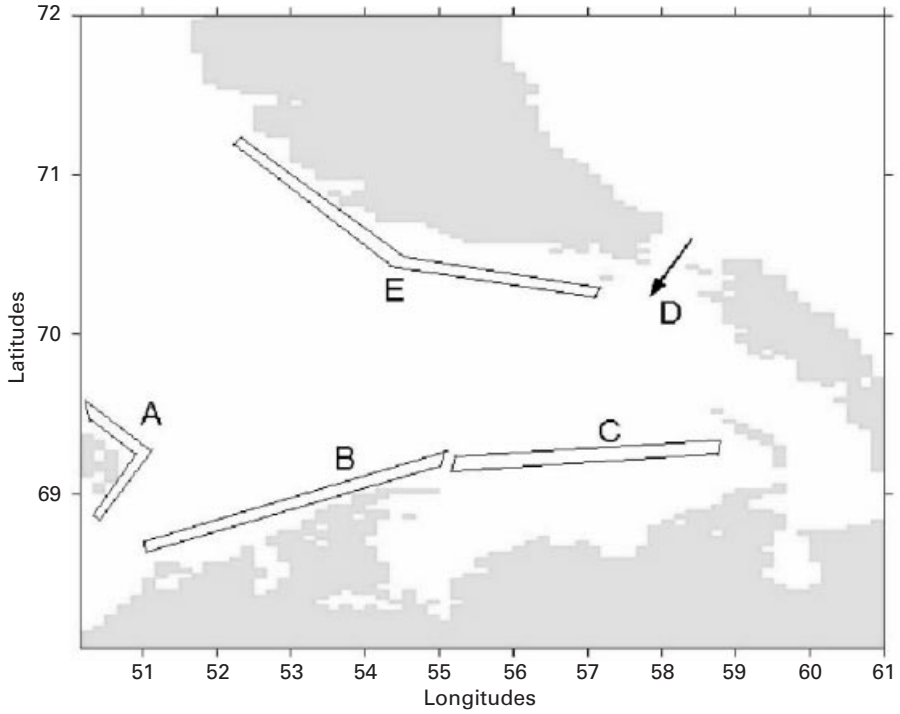

Figure 4. The start locations of ice ridges in the Pechora Sea.

The hit probability is divided into a global and a local probability. The global hit probability is defined as the probability of an ice ridge entering an area centred on the structure. The local hit probability is the probability that an ice ridge having entered the area will hit the structure; that is, enter a safety zone surrounding the structure.

The estimated number of ice ridges hitting the structure per year is obtained from:

$$E_N = P_l \times P_g \times N, \tag{12}$$

where: P_l and P_g are the local and global probabilities respectively, while N is the average number of ice ridges produced in the area of interest per year.

The size of the area used should reflect the uncertainty of the simulations performed. Poor quality in the simulations would claim a wide area and the opposite if the quality is good. The safety zone for an offshore structure would normally be one nautical mile or one hour of ice ridge drift, whichever is the least.

6.1. *Risk Analyses in the Pechora Sea.* The field used in this hit analysis has been the oil field Dolginskoye. Ice ridges starting from different positions in the Pechora Sea have been simulated, and the number of ridges entering an area of 10×10 km centred on an imaginary structure at Dolginskoye have been counted. The mean and maximum speeds of the ridges have been measured.

The ridges are assumed to have shapes as described in section 4, and the simulations were started from the five areas shown in Figure 4. The density of ridges in these waters is approximately as follows (Gudmestad *et al.*, 1999):

A. Kolguyev, 1–2 balls
B. Khodovarikha, 3–5 balls

https://doi.org/10.1017/S0373463300001144 Published online by Cambridge University Press

C. Varandey, 3–5 balls
D. Kara Gate, unknown.
E. Novaya Zemlya, 3–5 balls

Common for all starting positions was a water depth in the range of 15 to 25 m, i.e. in the shear zone. The ridges started from position D, the Kara Gate, and consisted of multi-year ice while the others consisted of first-year ice. No information was found on the number of ice ridges that start to drift in the Pechora Sea each year. In the Okhotsk sea, however, the average ridge length is about 500 m if the ridge extension is 1 ball and 144 m for 4 balls (Astafiev *et al*., 1997). The specific ice ridge length at the Prirazlomnoye field in April 1999 was 7·9 km/km^2 and near Varandey 5·4 km/km^2 (Pechora Sea, Ice Research Expedition 1999). This information was used together with the length of the coast and the average width of the shear zone to give some coarse estimates on the number of ridges in the Pechora Sea, Tables 2 and 3.

Table 2. Estimated number of ice ridges formed in the transition zone in the Pechora Sea per year.

Start position	(A) Kolguyev	(B) Khodovarihka	(C) Varandey	(D) Kara	(E) N.Z.	Total
No. of ridges	6600	52000	46000	1000*	27000	132600

* Not an estimate, only a suggested value.

Table 3. Probability that an ice ridge in the Pechora Sea is formed at various locations (in %).

Start position	(A) Kolguyev	(B) Khodovarihka	(C) Varandey	(D) Kara	(E) N.Z.
Number of hits	5·0	39·2	34·7	0·8	20·4

The ice period in the Pechora Sea lasts from the beginning of November to the end of July (Gudmestad *et al*., 1999). The ice ridge drift simulations have therefore been performed within these months. The fact that the ice regime will be different from the middle of the winter to the spring has not been accounted for. According to Romanov (1993), the ridges in the summer are being almost entirely melted down and therefore are not considered as a threat to offshore structures. The simulations were stopped if the ridges grounded or left the area of interest, i.e. the area shown in Figure 4. The forces used in the simulations were as described in Section 3. The ice ridge parameters needed, such as Length or Diameter, L or D, were found from the area distribution in Table 1.

The maximum sail height-h_s, was taken to be one metre in accordance with the ice ridge observed by Høyland and Løset (1999). This value is consistent with measurements from the Pechora Sea in 1999 when the average sail peak was measured as 1·8 m. (Pechora Sea, ice research expedition 1999).

The thickness of the consolidated layer – T_b, was given a value of two metres. This was based on the assumption that the consolidated ridge layer thickness is approximately twice as large as that for the level ice, and from Romanov (1993) that the level ice thickness during the winter in the Pechora Sea is approximately one metre.

6.2. *Local Hit Probability*. The local hit probability was determined from the simulation of 100 drift tracks for ice ridges within a 10 km × 10 km local area. The

https://doi.org/10.1017/S0373463300001144 Published online by Cambridge University Press

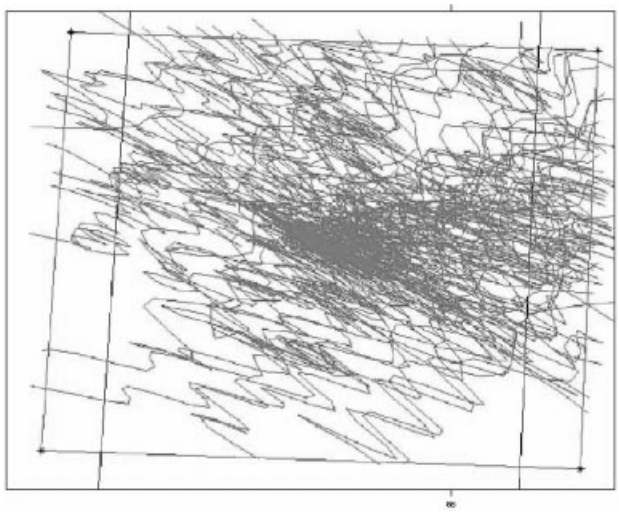

Figure 5. Track of 100 ice ridges simulated from Dolginskoye.

simulations were all started at the centre of the area and stopped if the ridges had drifted outside it. The start time of simulations was chosen randomly in the period between November 1 and May 30. The purpose of these simulations was to determine whether or not the ice movement was linear inside the square.

In order to determine the local probability, areas or windows of the same size were positioned arbitrarily along the simulated ice ridge tracks. Each segment of the tracks within such a window was analysed used a method applied for determination of the fractal dimensions of a curve in a two-dimensional space (Voss, 1988). The basis of this method is as follows:

(a) The square window is subdivided into smaller windows or boxes of size $L_b \times L_b$.
(b) The number of boxes containing a part of an ice ridge track is counted.
(c) The above procedure is repeated for diminishing box sizes. In this study, the smallest box size chosen was 1 km × 1 km.
(d) The number of boxes $N(L_b)$ versus box side is plotted on a log-log scale.

The fractal dimension D is defined as the (negative) slope of the $\log(N(L_b))$ versus $\log(L_b)$ line assuming that:

$$N(L_b) = C \times \left(\frac{L_b}{L_0}\right)^{-D}, \tag{13}$$

where: C is constant, and L_0 is a scaling factor.

Having established $N(L_b)$ from equation (13), the local hit probability $P(L_b) = P_l$ for an area of size $\Delta A = L_b \times L_b$ can be expressed by:

$$\begin{aligned} P(L_b) &= N(L_b) \times \left(\frac{\Delta A}{A}\right) \\ P(L_b) &= C \times \left(\frac{L_b}{L_0}\right)^{-D} \times \left(\frac{L_b^2}{k \cdot L_0^2}\right) \\ P(L_b) &= \left(\frac{C}{k}\right) \times \left(\frac{L_b}{L_0}\right)^{2-D} \end{aligned} \tag{14}$$

https://doi.org/10.1017/S0373463300001144 Published online by Cambridge University Press

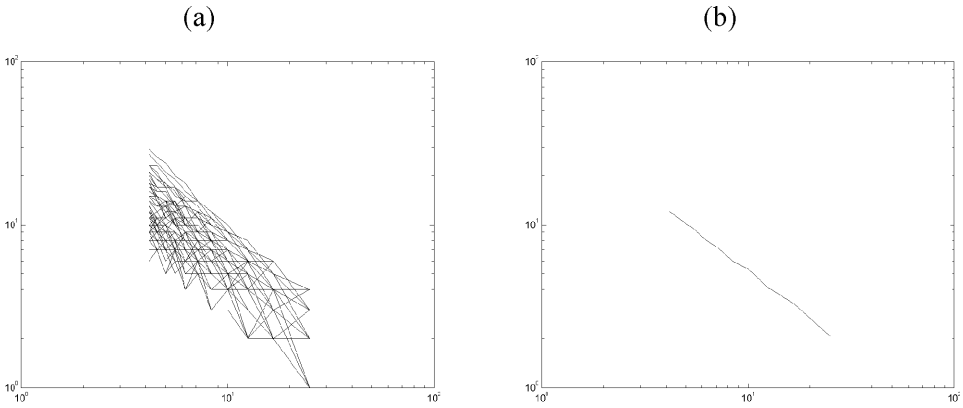

Figure 6.(a) Log(number of boxes) versus log(box size), (b) Mean value of tracks simulated.

Table 4. Local hit probability, i.e. the probability that an ice ridge having entered the 10 km × 10 km area centred at 69°30′N 55°30′E (at the centre of the Dolkinskoye field in the Pechora Sea) is to enter a box of size $L_b \times L_b$ within this area.

	Box size (L_b)		
	100 m	200 m	1000 m
Probability	6·75%	13·05%	61%

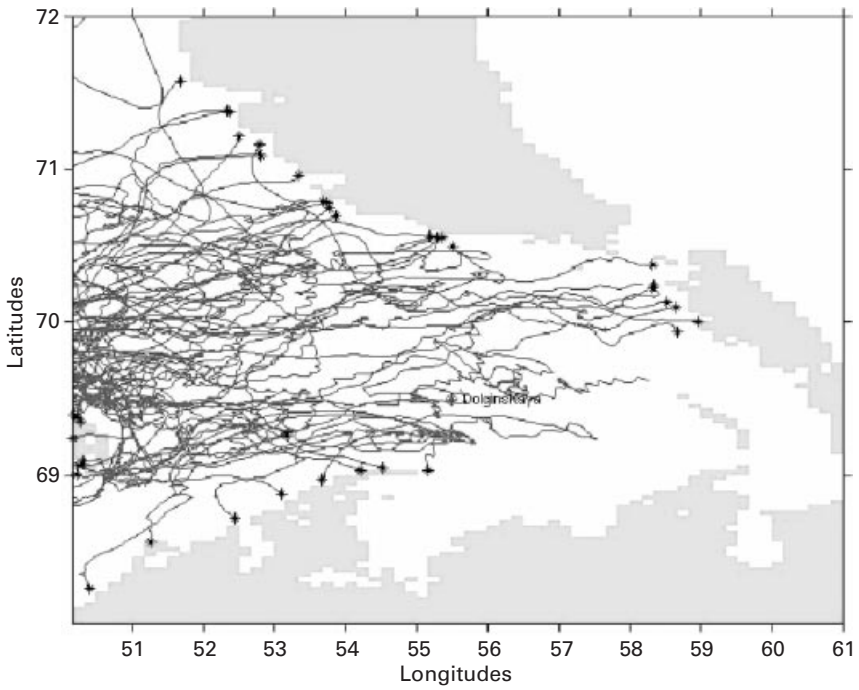

Figure 7. Simulations performed for the season 1987 to 1988. Started from Kolguyev, position A.

https://doi.org/10.1017/S0373463300001144 Published online by Cambridge University Press

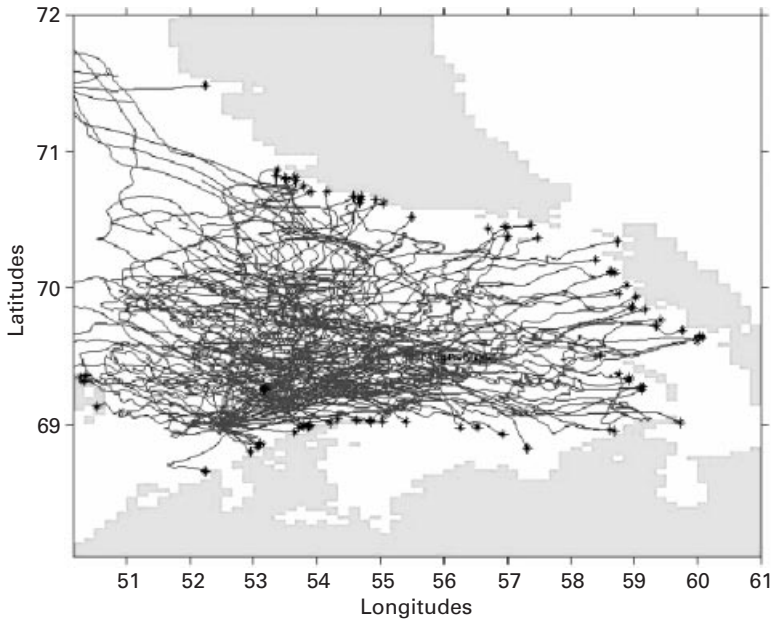

Figure 8. Simulations performed for the season 1987 to 1988. Started from Khodovarihka, position B.

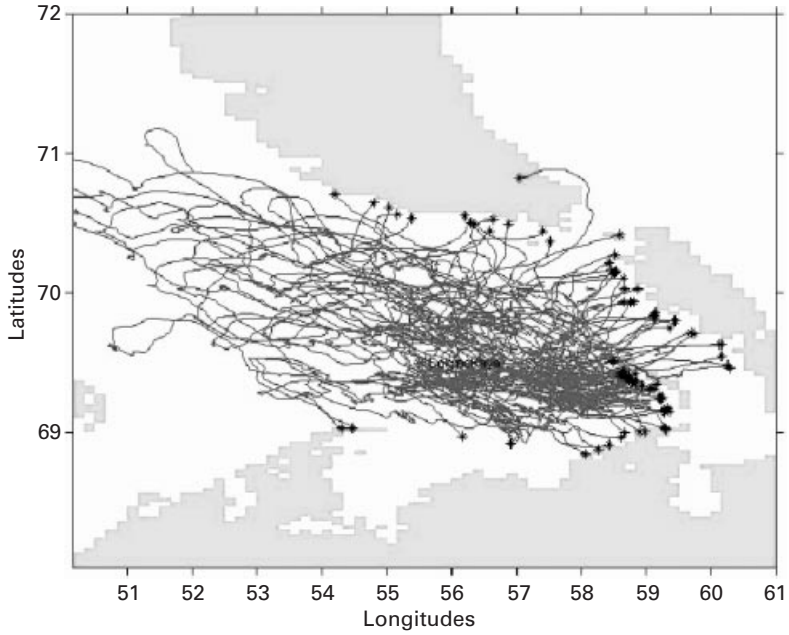

Figure 9. Simulations performed for the season 1987 to 1988. Started from Varandey More, position C.

https://doi.org/10.1017/S0373463300001144 Published online by Cambridge University Press

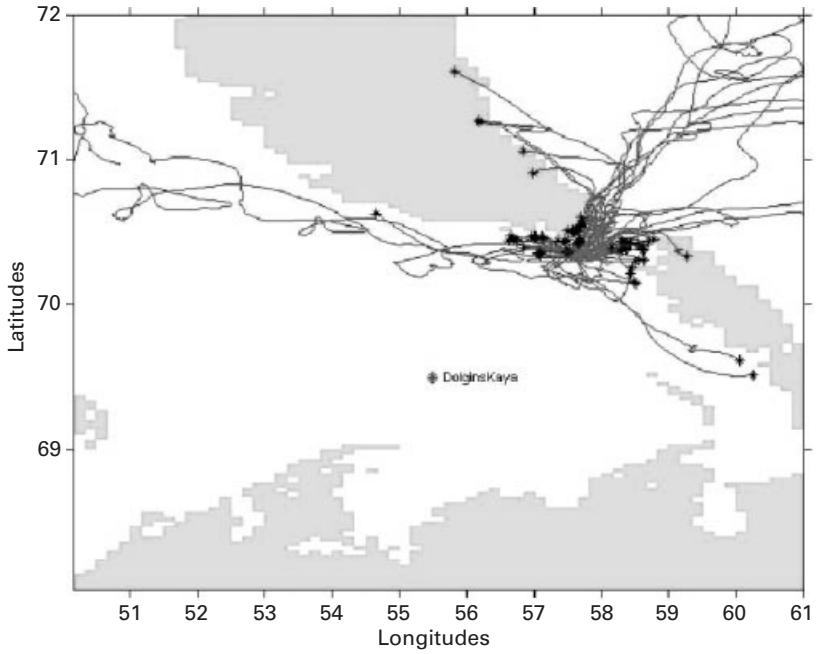

Figure 10. Simulations performed for the season 1987 to 1988. Started from the Kara Gate, position D.

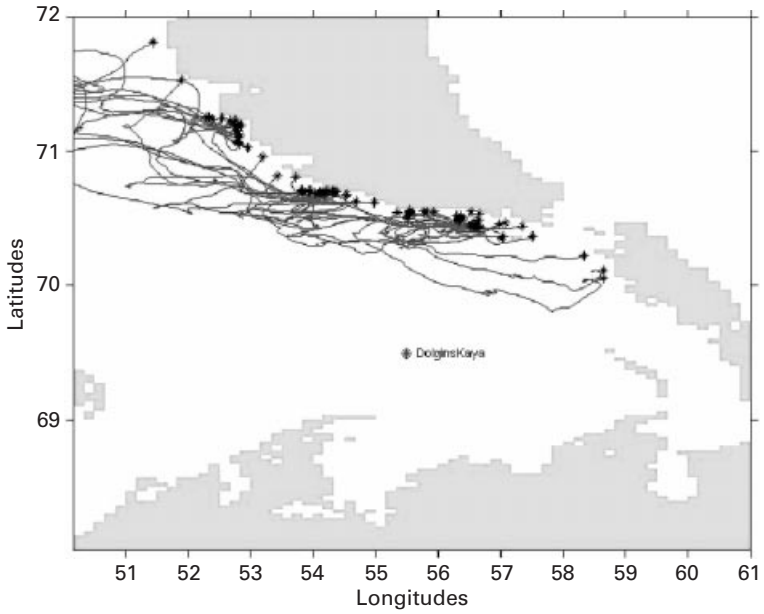

Figure 11. Simulations performed for the season 1987 to 1988. Started from Novaya Zemlja, position E.

https://doi.org/10.1017/S0373463300001144 Published online by Cambridge University Press

where: $A = k \cdot (L_0)^2$ is the size of the (10 km × 10 km) window area. For instance, if $L_0 = 1{\cdot}0$ km, $k = 10 \times 10 = 100$.

The 100 ice ridge drift tracks simulated for the computation of the local hit probability are shown in Figure 5. The plots of the number of boxes visited versus box size, $N(L_b)$ versus L_b, for these drift tracks are shown in Figure 6 (a), while Figure 6(b) shows the resulting weighted average $N(L)$ versus L relationship. By inspection of Figure 6 we see that $C = 61$ (provided that $L_0 = 1{\cdot}0$ km) and that $D = 1{\cdot}05$ Consequently, the local iceberg hit probability is given by:

$$P(L_b) = 0{\cdot}61 \times \left(\frac{L_b}{L_0}\right)^{0{\cdot}95} \quad \mathrm{L}_0 = 1{\cdot}0 \text{ km} \tag{15}$$

By inserting for different box sizes in the above formula we obtain the results as presented in Table 4.

6.3. *Global Hit Probability*. The simulations from the positions shown in Figure 4 were performed for the seasons 1987 to 1990. The results from the season 1987–88 are shown in the Figures 7 to 11. Grounded ridges are marked with a black star.

The number of ice ridges simulated from each position were 100 per year giving a total of 1500 simulated ice ridge trajectories in the Pechora Sea. Out of these ridges, 39 did enter the 10 km × 10 km area centred on the structure. As can be seen from the Figures 7 to 11 and from Table 5, most of these ridges started from Khodovarikha, position B.

Table 5. Number of ice ridges entering the 10 km × 10 km area centred at the structure sorted after the ice ridges origin.

Start position	(A) Kolguyev	(B) Khodovarihka	(C) Varandey	(D) Kara	(E) N.Z.
Number of hits	6	23	10	0	0

The mean drift speed during the computations was 0·21 m/s, and the maximum speed achieved was 0·89 m/s. This average speed is close to the findings by Løset and Onshuus (1999). Based on the analysis of four Argos positioned drift buoys deployed on the drift ice in the Pechora Sea, they estimated an average drift speed of 0·19 m/s. From the results in Table 5 and the estimates in Tables 2 and 3, the global probability of hit is 4·3 %.

$$P_g = 0{\cdot}05 \times \frac{6}{300} + 0{\cdot}392 \times \frac{23}{300} + 0{\cdot}347 \times \frac{10}{300} = 0{\cdot}0426 \approx 4{\cdot}3\,\%$$

By looking separately at the ridges simulated from Khodovarihka the probability of hitting the 10 km × 10 km area is found to be approximately 7·7 %.

$$P(Hit) = \frac{23}{300} = 0{\cdot}0767 \approx 7{\cdot}7\,\%.$$

It should be noted that the simulations show that it is likely that the ice ridges will ground offshore Varandey, near Dolgy islands and in the Kara gate. This is in accordance with observations (see Spichkin and Egorov (1995), and Losev and Gorbunov (1977).)

6.4. *Overall Ice Ridge Hit Risk*. The expected number of ice ridges reaching the Dolginskoye area per year is given by:

$$E_N = P_l \times P_g \times N$$

https://doi.org/10.1017/S0373463300001144 Published online by Cambridge University Press

where: P_l is the local hit probability and N the average number of ice ridges produced in the Pechora Sea per year.

If the local area is taken to be a 200 m × 200 m area centred at the structure, the local hit probability is $P_l = 13{\cdot}05\,\%$ as given in Table 4.

Since the estimates for the average number of ice ridges – N, produced in the Pechora Sea per year were very coarse, the expected number of ice ridges hitting a structure have been expressed as a function of annual production of ice ridges in the Pechora Sea, N, as given in Table 6.

Table 6. Expected number of hits between ice ridge and structure.

Annual number of ice ridges produced, N	50000	100000	132600	150000
Expected number of hits per year	278	556	737	834
Expected number of ridges entering the platform safety zone per year ($= P_g \times 1 \times N$)	2130	4260	5649	6390

7. DISCUSSION. The hit risk estimates found from the simulations are very uncertain, and conclusions based on the analyses of this work should not be relied upon. Nevertheless, the program ICEBERG has been developed to carry out hit analyses using the method presented in this paper. This makes it possible to perform new analyses easily and to calculate better hit risk estimates as soon as more information about the ice ridge regime in the Pechora Sea is available.

7.1. *The Drag Forces*. Both the wind drag force and water drag force are calculated by use of drag coefficients found for icebergs. A drag force will strongly depend on the shape of the body on which the wind/current is acting, and it is not likely that an ice ridge will cause the same disturbances as an iceberg.

By investigating the current in the waters where the simulations were performed, it was found that the tidal current contribution would be significant. Unfortunately, the tidal current model used has never been verified for the shallow waters in the Pechora Sea, and this represents the major uncertainty in the simulations performed.

7.2. *Assumptions made about the Ice Ridges*. The choice of a constant maximum sail height – h_s, and thickness of consolidated ice layer – $t_{b,}$ was made because of the lack of information about the distribution of these parameters. Observations of ridges with sail height higher than four metres (Golovin *et al*., 1996) indicate that there exist much larger ridges than used in this hit analysis. A statistical distribution for these two parameters, as for the surface area, would be recommended for use if available. The size and shape of the ice ridges have been constant during the simulations. This is done mainly due to lack of formulae for calculating the ice ridge melting terms.

7.3. *Bottom Topography*. The fact that the water level taken from a sea map is given for the lowest low-tide, implies that the water usually is deeper than assumed and that grounded ridges could have drifted significantly longer.

7.4. *The Hit Analysis*. The global hit analysis should have been performed over a much longer period with several more ice ridges started in different positions at different times. The number of ridges that are produced, the size of them, the prevailing wind and currents are known to be different from year to year, and simulations for only three years are not sufficient to take these variations into consideration.

8. CONCLUSIONS. The predominant ice drift direction during the winter months is to the northeast (November-May). If the model used for calculating tidal current is correct, the influence of tidal current on the ice ridge drift will be very strong. For the Dolginskoye field the following estimates can be given:

(a) The mean drift speed of the sea ridges was found to be 0·21 m/s with a maximum speed of 0·89 m/s.
(b) For a 200 m × 200 m wide structure, the expected number of hits per year was calculated to 737. It was assumed that a total number of 133000 sea ice ridges would be produced in (or have entered) the Pechora Sea per year. Under the same assumption the expected number of ridges entering a safety zone around the platform of 1852 m × 1852 m was found to be 5649.
(c) A structure located at Dolginskoye will most probably be exposed to sea ice ridges that are formed in the area around Khodovarihka.
(d) The ridge drift pattern shows a dominant drift towards northeast in the winter months.

These estimates are just indicative since there are many uncertainties in the input data such as ridge production/population, shapes, sizes and forcing. Thus a final conclusion about the expected annual number of hits cannot be drawn. The results of the simulations are, however, encouraging, suggesting that the method could be used to find the risk of hits between offshore structures and ice ridges accurately in the Pechora Sea.

REFERENCES

Arntsen, Ø., Løset, S. and McClimans, T. A. (1998). Naturlaster/Miljø VK, kompendium I faget 37083, NTNU. *Institute of Construction Technique*, p. 236 (in Norwegian).

Astafiev, V. N., Surkov G. A. and Truskov P. A. (1997). Ridges and Stamuchas of Okhotsk Sea. St. Petersburg. *Progress Pogoda*, p. 197.

Bigg, G. R., Wadley, M. R., Stevens, D. P. and Johnson, J. A., (1996). Prediction of the iceberg trajectories in the North Atlantic and Arctic Oceans. *Geophysical Research Letter* **23**, 3587–3590.

Bigg, G. R., Wadley, M. R., Stevens, D. P, and Johnson, J. A. (1997). Modelling the dynamics and thermodynamics of icebergs. *Journal of Cold Regions Science and Technology* **26**, pp. 113–135.

Chirivella, J. E. and Miller, C.-G. (1978) Hydrodynamics of icebergs in transit. *Proceedings of the First Conference on Iceberg Utilization for Freshwater Production*. Iowa State University, pp. 315–333.

Gjevik, B., Nøst, E. and Straume, T. (1990) Atlas of tides on the shelves of the Norwegian and the Barents Seas. *Department of Mathematics*, *University of Oslo*. p. 9.

Golovin, N. V., Koptev, N. S., Maiorov, O. N. and Khvedynych (1996). The ice investigations in the Pechora and Kara Seas. *Proceedings of the Polar. Tech. Conference*, St. Petersburg, 1996, Vol. **4**, pp. 38–39.

Gudmestad, O. T., Zolotukhin, A. B., Ermakov, A. I., Jakobsen, R. A., Michtchenko, I. T., Vovk, V. S., Løset, S. and Shkhinek, K. N. (1999) *Basics of Offshore Petroleum Engineering and Development of Marine Facilities*. Stavanger, Moscow, St Petersburg, Trondheim, 1999, p. 344.

Høyland, K. W. and Løset, S. (1999). Measurements of temperature distribution, consolidation and morphology of a first-year sea ice ridge. *Cold Regions Science and Technology*, Vol. **29**, pp. 59–74.

Johannessen, K. (1998). *Simulation of Iceberg Drift*. Thesis, summer 1998, Statoil, p. 45.

Losev, S. M. and Gorbunov Y. A. (1977). *Studying of Stamuchas according to Aerophotographs*. Tr. AANII, t. 343, pp. 127–132.

Løset, S. and Onshuus, D. (1999). Analysis of speeds of drift ice in the Pechora Sea. *Proceeding of the* 4^{th} *International Conference Development of the Russian Arctic Offshore* (*RAO*'99), St. Petersburg, July 6–9, 1999, Vol. I, pp. 248–253.

Mathiesen, M., Løvås, S. M. and Vefsnmo, S. (1992). Iceberg Collision – Risk Analyses. SINTEF-NHL, *Report STF*60 *F*92047.

Neumann, G. and Pierson, W. J. (1966). *Principles of Physical Oceanography*. Prentice Hall Inc., Englewood Cliffs, N. J., USA, p. 545.

Romanov, I. P. (1993). *Ice Cover of the Arctic Basin*. Draft, p192.

Slagstad, D. and Wassmann, P. (1995). Climate change and carbon flux in the Barents Sea: 3-D simulations of ice-distribution, primary production and vertical export of particulate organic carbon. *Proceedings of the International Symposium on Environmental Research in The Arctic* 1995, pp. 119–141.

Smith, S. D. (1993). Hindcasting iceberg drift using current profiles and winds. *Journal of Cold Regions Science and Technology* **22**, pp. 33–45.

Spichkin, V. and Egorov, A. (1995). Dangerous ice phenomena in the Barents and Kara Seas offshore. *Proceedings of the Second International Conference on Development of the Russian Arctic Offshore* (*RAO-*95), St. Petersburg, 1995.

Timco, G. W. and Burden, R. P. (1996). An analysis of the shapes of sea ice ridges. *Journal of Cold Regions Science and Technology* **25** (1997), pp. 65–77.

Voss, R. F. (1988). Fractals in nature – from characterization to simulation. Pp. 21–70. In: Peitgen, H. O. and Saupe, D., *The Science of Fractal Images*. Springer Verlag, New York, pp. 312.

Technical Report (1999). Pechora Sea 1999 Ice Research Expedition. *The Arctic and Antartic Research Institute* (*AARI*), p. 175.